Published in final edited form as:

FASEB J. 2023 November ; 37(11): e23251. doi:10.1096/fj.202301122RR.

Targeting phospholipid remodeling pathway improves insulin resistance in diabetic mouse models

Ye Tian[1], **Wei Lu**[1], **Ruicheng Shi**[1], **Reagan McGuffee**[4], **Richard Lee**[5], **David A. Ford**[4], **Bo Wang**[1,2,3,*]

[1]Department of Comparative Biosciences, College of Veterinary Medicine, University of Illinois at Urbana-Champaign, Urbana, IL, USA

[2]Division of Nutritional Sciences, College of Agricultural, Consumer and Environmental Sciences, University of Illinois at Urbana-Champaign, Urbana, IL, USA

[3]Cancer Center at Illinois, University of Illinois at Urbana-Champaign, Urbana, IL, USA

[4]Department of Biochemistry and Molecular Biology, and Center for Cardiovascular Research, Saint Louis University, St. Louis, MO, USA, 63104

[5]Ionis Pharmaceuticals, Carlsbad, CA, USA.

Abstract

Previous studies have revealed that membrane phospholipid composition controlled by lysophosphatidylcholine acyltransferase 3 (LPCAT3) is involved in the development of insulin resistance in type 2 diabetes. In this study, we aimed to investigate the therapeutic potential of targeting *Lpcat3* in the treatment of insulin resistance in diabetic mouse models. *Lpcat3* expression was suppressed in the whole body by antisense oligonucleotides (ASO) injection or in the liver by adeno-associated virus (AAV)-encoded Cre in high-fat diet (HFD)-induced and genetic *ob/ob* type 2 diabetic mouse models. Glucose tolerance test (GTT), insulin tolerance test (ITT), fasting blood glucose and insulin levels were used to assess insulin sensitivity. Lipid levels in the liver and serum were measured. The expression of genes involved in *de novo* lipogenesis was analyzed by real-time RT-PCR. Metabolic rates were measured by indirect calorimetry using the Comprehensive Lab Animal Monitoring System (CLAMS). Our data demonstrate that acute knockout of hepatic *Lpcat3* by AAV-Cre improves both hyperglycemia and hypertriglyceridemia in HFD-fed mice. Similarly, whole body ablation of *Lpcat3* by ASO administration improves obesity and insulin resistance in both HFD-fed and *ob/ob* mice. These findings demonstrate that targeting LPCAT3 could be a novel therapy for insulin resistance.

Graphical Abstract

*Correspondence: Bo Wang, Ph.D. Department of Comparative Biosciences, College of Veterinary Medicine, University of Illinois at Urbana-Champaign, Urbana, IL, USA bowang@illinois.edu, 1-217-300-8084.

Author contributions. Y.T. designed and performed experiments, analyzed data, and wrote the paper. W.L. and R.S. performed experiments and analyzed data. R.M. and D.A.F. performed phospholipid quantification and analyzed data. R. L. provided access to, and expertise pertaining to ASO generation and delivery. B.W. conceived the project, designed experiments, analyzed data, supervised the project, and wrote the paper.

Conflict of interest. R. L. holds shares in Verve Therapeutics. All other authors declare no competing interests related to this work.

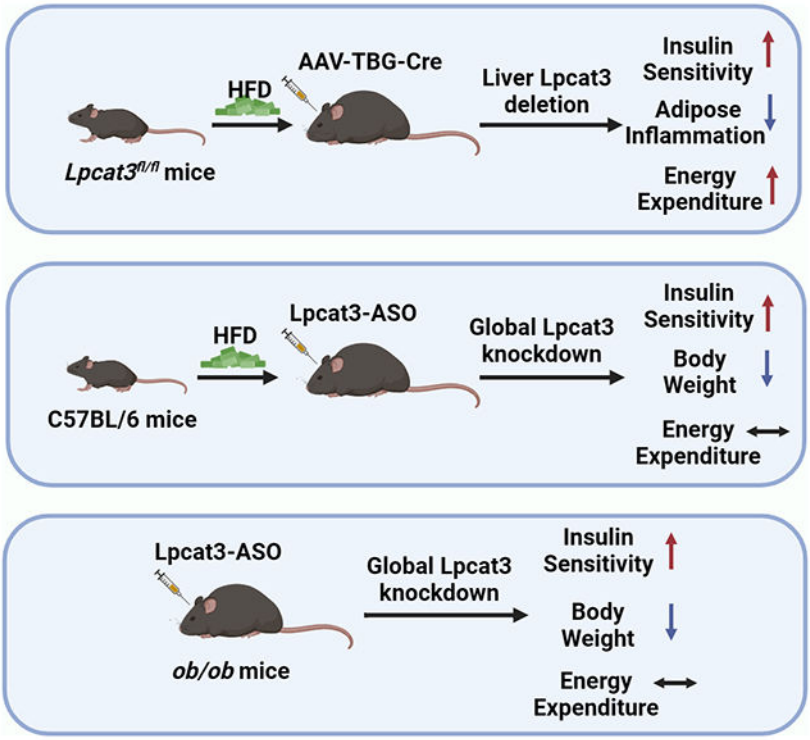

Deletion of Lpcat3 in the liver or whole-body suppression of Lpcat3 expression through antisense oligonucleotides (ASO) treatment improves obesity and insulin sensitivity in both high-fat diet-induced and genetic *ob/ob* mouse models.

Keywords

Type 2 diabetes; insulin resistance; obesity; LPCAT3; phospholipid remodeling

Introduction

In 2021, diabetes is estimated to affect approximately 500 million people worldwide, with about 90% of them having type 2 diabetes (1), which has become one of the fastest growing health concerns of the century (2, 3). Insulin resistance is a major risk factor for type 2 diabetes comorbidities, including hypertriglyceridemia. This is mainly driven by the defective glucose production suppression combined with intact promotion of lipogenesis upon insulin signaling in the liver, also known as selective insulin resistance (4–6). This paradoxical effect dampens the therapeutic efficacy of insulin due to increased lipid production, necessitating further investigation into its pathology.

Phospholipids are major constituents of biological membranes, and their fatty acyl chains exhibit high levels of diversity in length and degree of saturation. These characteristics of phospholipids not only determine the biological properties of membranes, but also influence membrane-associated processes, thereby playing a crucial role in regulating pathophysiological conditions (7, 8). In mammalian cells, phospholipid composition is

primarily maintained through the Lands' cycle, a remodeling process of de-acylation and re-acylation (9). Lysophosphatidylcholine acyltransferases 3(LPCAT3) is an enzyme highly expressed in the liver, intestine, and adipose tissues that preferentially incorporates polyunsaturated fatty acyl chain into the sn-2 site of lysophospholipids (10, 11). Recent studies have highlighted the crucial roles of membrane phospholipid composition in the regulation of metabolism. LPCAT3 has been shown to maintain lipid homeostasis by controlling the lipidation and secretion of very-low-density lipoprotein (VLDL) and chylomicron in the liver and intestine, respectively (12, 13). *Lpcat3* deficiency blunts SREBP-1c activation and lipogenic gene expression in the liver (14). Interestingly, LPCAT3 and phospholipid remodeling also play a role in regulating glucose metabolism and contributing to the development of insulin resistance in type 2 diabetes. It has been shown that *Lpcat3* expression and the levels of polyunsaturated phospholipids are increased in the livers of high fat diet (HFD)-fed and *ob/ob* mice (14, 15), two well established models of insulin resistance. Furthermore, deletion of *Lpcat3* in the liver significantly improves hepatic insulin resistance and systemic metabolism. Mechanistically, hepatic *Lpcat3* deficiency enhances insulin signal transduction by promoting insulin receptor endocytosis and increases energy expenditure by inducing FGF21 secretion (15). In the muscle, LPCAT3 affects insulin sensitivity by modulating plasma membrane lipid organization and insulin receptor phosphorylation (16). These findings suggest that *Lpcat3* could be a novel target to treat insulin resistance.

In this study, we tested the therapeutic potential of targeting *Lpcat3* using ASO- and adeno-associated virus (AAV)-mediated suppression of *Lpcat3* in diabetic mouse models. We showed that acute knockout of *Lpcat3* in the liver using AAV improves hyperglycemia and hypertriglyceridemia in mice fed a high-fat diet. Treatment with ASO to ablate *Lpcat3* effectively mitigates obesity and insulin resistance in both HFD-fed and *ob/ob* mice. These findings suggest that targeting *Lpcat3* and phospholipid remodeling could provide a promising therapeutic strategy for insulin resistance in type 2 diabetes.

Materials and Methods

Animals

All animal procedures were conducted in compliance with protocols approved by the Institutional Animal Care and Use Committee (IACUC) at University of Illinois at Urbana-Champaign (UIUC). *Lpcat3*$^{fl/fl}$ mice have been described before (12). *ob/ob* mice were acquired from the Jackson Laboratory. All mice were housed under pathogen-free conditions in a temperature-controlled room with a 12 h light/dark cycle. Mice were fed chow diet (LabDiet #5001) or high-fat diet (Research Diets #D12492). All experiments were performed with male mice unless otherwise stated. For RNA analysis, liver tissues were collected and snap frozen in liquid nitrogen and stored at −80°C. For food intake measurement, mice were housed individually in cages and food weight was measured daily. Mouse blood was collected by retro-orbital bleeding under anesthesia before sacrificing or by tail bleeding, and plasma was obtained by centrifugation. Plasma insulin levels were measured using Insulin ELISA kit (Crystal Chem).

Glucose and insulin tolerance test

Mice were fasted for at least 5 h in the morning and intraperitoneally (i.p.) injected with glucose or insulin (Novolin N, Human). Glucose was given at 1 g/kg body weight (BW) diluted in PBS. Insulin was given at 0.5 U/kg BW for chow diet-fed mice and 1 U/kg BW for HFD-fed and *ob/ob* mice. Blood glucose levels were measured from tail bleeding using a glucometer (OneTouch Ultra2) at designated time points.

Indirect calorimetry and body composition measurements

Metabolic rates were measured by indirect calorimetry in open-circuit Oxymax chambers in the Comprehensive Lab Animal Monitoring System (CLAMS) (Columbus Instruments). Mice were housed individually in the chamber, and O_2 gas was calibrated before monitoring. The chamber was maintained at 23°C with 12-hour light/12-hour dark cycles, and food and water were available ad libitum. O_2 consumption and CO_2 production were measured directly as continuously accumulated data. Energy expenditure (EE) was calculated as $(3.815+1.232*RER)*VO_2$ and linear regression analysis of covariance (ANCOVA) was used to determine mass-independent effect between F/F and LKO mice as reported before (17, 18). Estimated EE was calculated by univariate generalized linear model (GLM) with body mass set to the average of both treatment groups. Body composition (whole-body fat and lean mass) was determined using Echo MRI Body Composition Analyzer.

Histology

Tissues were collected, fixed in 10% buffered formalin, embedded in paraffin, sectioned at 4–10 μm and stained with hematoxylin and eosin at the University of Illinois Histology Lab.

Gene expression analysis

Total RNA was isolated from tissues with Trizol (Invitrogen), cDNA was synthesized, and gene expression was quantified by BioRad CFX384 Touch Real-Time PCR Detection System with SYBR Green (BioRad). For ASO injected mice, total RNA was isolated with Direct-zol RNA Kits (Zymo Research), and cDNA was synthesized using iScript™ cDNA Synthesis Kit (BioRad).

Protein analysis

For *in vivo* insulin signaling, insulin (Novolin N, Human) was injected to overnight fasted mice retro-orbitally. Then, the liver, muscle, and adipose tissues were harvested 10 min post insulin injection. phospho-AKT levels were assessed by Western blot analysis in tissue lysates as described (19). Briefly, tissues were homogenized and sonicated in RIPA buffer (50 mM Tris–HCl, pH 7.4, 150 mM NaCl, 0.1% Triton X-100, 0.5% sodium deoxycholate, 0.1% SDS) supplemented with protease inhibitors (Roche Molecular Biochemicals) and phosphatase inhibitors (Sigma Aldrich). The homogenate was then cleared by centrifugation. After quantifying protein concentration using BCA kits (Thermo Fisher Scientific), 25 μg of proteins were mixed with sample buffer (BioRad), loaded to 4%−15% precast gel (BioRad) for electrophoresis and transferred to PVDF membranes (Amersham International, GE Healthcare). Membranes were then blocked with blocking buffer (5% BSA in 0.1% TBST) for 1 h at room temperature and then incubated with primary antibodies at 4°C overnight

diluted in blocking buffer. After washed with 0.1% TBST for 4 times, membranes were incubated with secondary antibodies diluted in blocking buffer for 1 h at room temperature. Membranes were developed using ECL western blotting substrate (Thermo Scientific) and were exposed to X-ray film (FUJI) in dark room.

Postprandial lipid absorption assay

Lipid absorption assay was performed as previously described (20). Briefly, mice were fasted for 4 h and gavaged with corn oil (10 μg/g body weight). Plasma was collected through tail vein at 0, 1, 2, 4 and 6 h and plasma lipids were measured with Wako triglyceride kit.

Lipid extraction and measurement

Liver tissues were snap-frozen in liquid nitrogen at the time of harvest. To extract lipids, liver tissues were cut, weighed and homogenized in water. After transferring the homogenate into glass tubes, lipids were extracted by adding 2 mL chloroform/methanol (2:1 v/v), mixed thoroughly by vortexing and centrifuged at 3,000 r.p.m. for 5 min at 4°C. Lipids in the lower layer were then carefully collected and air-dried overnight. The lipids were dissolved in ethanol and diluted in PBS for lipid measurements. Serum was directly used for lipid measurements. Serum and hepatic lipids were measured with the Wako L-Type TG M kit and the Wako HR series NEFA- HR(2) kit.

Phospholipid analyses

Mouse tissues were snap-frozen in liquid nitrogen. Tissues were homogenized on ice in phosphate buffered saline. Homogenates were subsequently subjected to a modified Bligh-Dyer lipid extraction (21) in the presence of lipid class internal standards, including 1–0-heptadecanoyl-sn-glycero-3-phosphocholine, 1,2-dieicosanoyl-sn-glycero-3-phosphocholine (22). Lipid extracts were diluted in methanol/chloroform (4/1, vol/vol), and molecular species were quantified using electrospray ionization mass spectrometry on a triple quadrupole instrument (Themo Fisher Quantum Ultra) employing shotgun lipidomic methodologies (23). Phosphatidylcholine (PC) molecular species were quantified as chlorinated adducts in the negative ion mode using neutral loss scanning for 50 amu (collision energy = 24 eV). Individual molecular species were quantified by comparing the ion intensities of the individual molecular species to that of the lipid class internal standard with additional corrections for type I and type II 13C isotope effects (23).

Antisense oligonucleotide (ASO) treatment

For acute ASO studies, C57BL/6 mice fed with HFD for 8 weeks or *ob/ob* mice at 6–7 weeks of age were subcutaneously injected with either control or *Lpcat3* ASO (GTACATAGTAGGCTTG) at 25 mg/kg twice per week for 4–5 weeks. Body weight was monitored weekly, and body composition was measured by Echo MRI analysis. GTT and ITT were performed on weeks 3 and 4. At the end of ASO treatment, tissues were resected and subjected to gene expression analysis.

Adeno-associated virus (AAV) mediated liver specific *Lpcat3* knockout

For liver-specific acute knockout of *Lpcat3*, *Lpcat3* $^{fl/fl}$ mice fed with HFD for 8 weeks were retro-orbitally injected with 1×10^{11} GC/mouse either AAV8-TBG-iCre (VB1724, Vector Biolabs) or control virus AAV8-TBG-GFP (VB1743, Vector Biolabs) in 100 μL saline under anesthesia. Mice were then continued to be fed with HFD for 4 weeks to characterize metabolic features.

Statistical analysis

For all studies, results from quantitative experiments were expressed as means ± SEM. GraphPad Prism 9.0 (San Diego, CA) was used for all statistical analyses. Where appropriate, significance was calculated by Student's t test, one- or two-way ANOVA with Tukey's or Sidak's multiple comparison test.

Results

Acute deletion of *Lpcat3* in the liver ameliorates insulin resistance in HFD-fed mice

Our previous studies have demonstrated that *Lpcat3* expression in the liver is induced by insulin and increased polyunsaturated PC levels contribute to the development of selective insulin resistance (15). To determine if targeting *Lpcat3* expression in the liver could improve hyperglycemia and hypertriglyceridemia, we fed *Lpcat3* floxed mice with HFD for 8 weeks and retro-orbitally injected mice with either an AAV8 expressing the codon improved Cre recombinase driven by liver-specific promoter TBG (AAV8-TBG-iCre) or a control AAV encoding eGFP (AAV8-TBG-eGFP). Both groups of mice exhibited similar body weight gain and body composition 4 weeks after the viral injection (Figure 1A–1C). Realtime RT-PCR confirmed liver specific knockout of *Lpcat3* upon AAV injection (Figure 1D). Intraperitoneal glucose tolerance test (IPGTT) showed that Cre-injected mice cleared glucose load more efficiently than eGFP-injected control mice (Figure 1E–1F). Insulin tolerance test (ITT) demonstrated that Cre-injected mice were slightly more insulin sensitive compared to controls (Figure 1G–1H). Furthermore, acute knockout of *Lpcat3* significantly reduced fasting blood glucose levels (Figure 1I), while no differences in serum insulin levels and HOMA-IR were observed (Figure 1J–1K).

It has been shown that *Lpcat3* deficiency suppresses lipogenesis and VLDL secretion in the liver (12, 14). Indeed, gene expression analysis showed that acute knockout of *Lpcat3* decreased the expression of SREBP-1c and its downstream lipogenic targets (Figure 2A). Serum triglyceride levels were markedly reduced with a concomitant increase in hepatic lipid accumulation upon *Lpcat3* deletion (Figure 2B–2E). Histology analysis revealed less inflammation in WAT, especially in epididymal white adipose tissue (eWAT) of Cre injected mice (Figure 2F). Consistent with our previous report, acute knockout of *Lpcat3* increased energy expenditure during dark cycle (Figure 2G–I), while food consumption, physical activity and respiratory exchange ratio (RER) were not affected (Figure 2J–2L).

Whole-body silencing of *Lpcat3* improves HFD-induced obesity and insulin resistance

Next, we investigated the effect of global suppression of *Lpcat3* on insulin sensitivity and lipid metabolism. We first subcutaneously injected chow diet-fed C57BL/6 mice with ASO

targeting *Lpcat3* (*Lpcat3*-ASO) or control ASO (Con-ASO) twice per week for two weeks and measured the knockdown efficiency in different tissues. Realtime RT-PCR analysis showed marked inhibition of *Lpcat3* expression in several metabolic organs, including liver, intestine, muscle and adipose tissues (Figure 3A). Next, we fed C57BL/6 mice with HFD for 8 weeks and subcutaneously injected ASOs for another 5 weeks. *Lpcat3* suppression resulted in a gradual decrease in body weight (Figure 3B). Next, we evaluated insulin sensitivity through glucose and insulin tolerance tests before any significant differences in their body weights emerged. Similar to chronic or acute liver-specific *Lpcat3* knockout (LKO), global suppression of *Lpcat3* expression significantly improved glucose intolerance and insulin resistance (Figure 3C–3H), and dramatically lowered fasting blood glucose levels, serum insulin levels and HOMA-IR (Figure 3I–3K). The final body weight showed a ~15% decrease in mice injected with Lpcat3-ASO, primarily in adipose tissues (Figure 3L–3N). We previously have shown that *Lpcat3* deficiency in the intestine suppresses food intake on HFD (13). However, at 5-week post ASO injection, we did not observe any significant difference in food intake between *Lpcat3*- and Con-ASO injected mice (Figure 3O), likely because the mice have adapted to HFD over time.

In contrast to LKO mice, which displayed reduced serum lipid levels accompanied by hepatic lipid accumulation (Figure 2B–2E), we found no differences in serum or hepatic triglyceride and NEFA levels were observed between Con-ASO and *Lpcat3*-ASO treated mice (Figure 4A–4D), despite a marked reduction in the expression of SREBP-1c and lipogenic genes (Figure 4E). Our previous studies have demonstrated that loss of *Lpcat3* in the intestine impairs lipid absorption (13). Indeed, mice treated with Lpcat3-ASO showed a trend toward reduced lipid output when subjected to oil gavage (Figure 4F), which may explain the absence of lipid accumulation in the liver. Histological analysis showed no overt difference in the liver and adipose tissues between control and *Lpcat3* ASO injected mice (Figure 4G). Metabolic rate analysis did not show any difference in energy expenditure or physical activity (Figure 4H–4K). However, *Lpcat3*-ASO injected mice exhibited a decrease in RER (Figure 4L), suggesting a higher utilization of fat as the body's primary fuel source. This shift in fuel utilization may contribute to the reduced adipose tissue weight and the absence of overt hepatic lipid accumulation in these mice.

ASO-mediated knockdown of *Lpcat3* increases membrane saturation and enhances insulin signaling

Our previous studies have revealed that *Lpcat3* deficiency in the liver improves insulin sensitivity through both cell-autonomous mechanisms involving increased membrane saturation and improved insulin signal transduction, and cell-nonautonomous mechanisms, driven by enhanced FGF21 secretion (15). Gene expression analysis showed a marked reduction in *Lpcat3* expression in metabolic organs, including liver, muscle, adipose tissues, following ASO treatment in HFD fed mice (Figure 5A). Phospholipid analysis revealed substantial alterations in PC composition in the liver, similar to the changes observed in LKO livers, characterized by a decrease in arachidonoyl-containing PCs and an increase in saturated and monosaturated PCs (Figure 5B). In contrast, the PC composition in muscle and adipose tissues was less affected (Figure 5C–E), showing only slight increases in monosaturated PCs and modest decreases in arachidonoyl-containing PCs. In line with our

findings in LKO mice, we observed a ~3-fold increase in serum FGF21 levels in mice treated with Lpcat3-ASO (Figure 5F). Western blot analysis showed a slight elevation in pAKT levels in the liver and BAT of mice treated with Lpcat3-ASO compared to those treated with Con-ASO (Figure 6A–D), indicating enhanced insulin signaling.

Global suppression of *Lpcat3* ameliorates obesity and insulin resistance in *ob/ob* mice

Next, we examined how global knockdown of *Lpcat3* affects metabolism in a genetically obese mouse model. Starting at 6 weeks old, *ob/ob* mice were subcutaneously injected with control or *Lpcat3* targeting ASO twice per week for 5 weeks. Similar to HFD-fed mice, *Lpcat3*-ASO treatment reduced body weight gain in *ob/ob* mice with a significant decrease in adipose tissue weight (Figure 7A–7D). Mice injected with Con- and *Lpcat3*-ASO had comparable food consumption (Figure 7E), indicating that the body weight difference was not caused by a difference in energy intake. GTT and ITT analysis in mice with comparable body weight showed significant improvement in glucose tolerance and insulin sensitivity in *Lpcat3*-ASO injected mice (Figure 7F–7K). Moreover, *Lpcat3*-ASO injected mice had lower fasting blood glucose, serum insulin levels and HOMA-IR than Con-ASO injected mice (Figure 7L–7N).

Whole-body suppression of *Lpcat3* expression had no effect on serum triglyceride and NEFA levels or hepatic NEFA levels, but significantly decreased hepatic triglyceride levels (Figure 8A–8D), which was likely a result of decreased expression of lipogenic genes in the liver (Figure 8E). Histology analysis also showed less lipid accumulation in the liver, while no difference in the histology of adipose tissues was observed (Figure 8F). CLAMS analysis revealed a slight increase in energy expenditure in *Lpcat3*-ASO injected *ob/ob* mice during light cycle (Figure 8G–8I), while physical activity was not different between groups (Figure 8J). Interestingly, there was a significant reduction in RER in *Lpcat3*-ASO injected mice (Figure 8K), suggesting that fat was utilized more as an energy source. Furthermore, the expression of lipases was significantly enhanced in the adipose tissues of *Lpcat3*-ASO injected mice (Figure 8L). Thus, reduced RER and increased lipase expression may contribute to smaller fat depots in *Lpcat3*-ASO injected mice.

Discussion

Phospholipid composition in biological membranes has been increasingly recognized to have significant impact on normal physiological processes and pathological conditions. In previous studies, we have demonstrated that LPCAT3 and phospholipid remodeling are involved in the regulation of VLDL secretion (12), SREBP-1c-mediated lipogenesis in the liver (14), and chylomicron metabolism in the intestine in normal physiology (13). Our recent investigations have further revealed the involvement of LPCAT3 in the development of disease conditions (15, 19), including selective insulin resistance in type 2 diabetes. Specifically, we have found that hyperinsulinemia increases hepatic *Lpcat3* expression and polyunsaturated PC levels, and that chronic *Lpcat3* deficiency in the liver improves insulin sensitivity in both HFD-fed and genetic *ob/ob* mouse models. In this study we show that acute targeting of *Lpcat3* in the liver through AAV-Cre mediated knockout or whole body *Lpcat3* knockdown via ASO injection improve insulin resistance in both HFD-fed and *ob/ob*

mice. These studies provide a proof of concept that manipulating *LPCAT3* expression and membrane phospholipid composition could be a potential therapeutic strategy for treating insulin resistance in type 2 diabetes.

The pathogenesis of insulin resistance involves multiple metabolic organs, including liver, muscle and adipose tissues (24–27). Insulin signaling regulates glucose homeostasis by suppressing glucose production in the liver and enhancing glucose uptake in the muscle and adipose tissues. Interestingly, we and others have demonstrated that LPCAT3 and phospholipid composition modulate insulin signaling and glucose metabolism in both the liver and muscle (15, 16). Loss of *Lpcat3* in the liver improves insulin sensitivity through both cell autonomous and nonautonomous effects. Increasing membrane phospholipid saturation facilitates insulin receptor internalization and downstream signal transduction, and increases FGF21 secretion and glucose uptake in brown adipose tissues (15). Similarly, *Lpcat3* deficiency in the muscle enhances insulin sensitivity by increasing membrane lipid clustering and potentiating insulin action (16). Although it is unclear whether phospholipid remodeling affects insulin signaling and glucose uptake in adipose tissue, we believe that the improved insulin sensitivity in ASO treated mice could be attributed, at least partially, to the effects of *Lpcat3* suppression in both the liver and muscle.

It is well established that hyperinsulinemia activates SREBP-1c, leading to enhanced lipogenesis, but fails to suppress glucose production in the livers of type 2 diabetic patients, a phenomenon referred to as selective insulin resistance (4, 28). Our studies have shown that LPCAT3 and membrane unsaturation mediate both lipid promoting and anti-glucose producing effects of insulin. Thus, we anticipate that inhibiting *Lpcat3* could improve both hyperglycemia and hypertriglyceridemia in HFD-induced or genetic ob/ob insulin resistant models. Indeed, acute knockout of *Lpcat3* by AAV-Cre injection lowered both blood glucose and triglyceride levels. Similarly, ASO treatment in HFD-fed and *ob/ob* mice also resulted in decreased blood glucose levels. We also observed a marked reduction in hepatic triglyceride levels in *ob/ob* mice. Surprisingly, serum triglyceride levels were not affected after ASO treatment, despite the significant suppression of SREBP-1c expression and its downstream targets involved in lipid *de novo* synthesis in ASO treated livers. We reason that altered lipid metabolism resulting from *Lpcat3* knockdown in other organs, such as adipose tissue and intestine, may have obscured the effect of *Lpcat3* suppression on hepatic lipid metabolism. Indeed, thanks to the reduced lipid absorption caused by the suppression of *Lpcat3* in the intestine, HFD-fed mice treated with ASO showed no discernible difference in hepatic triglyceride levels compared to controls. This observation implies that ASO-mediated whole body *Lpcat3* knockdown mitigated the development of steatosis in mice with hepatic specific *Lpcat3* knockout, enhancing the potential of ASO treatment as a therapeutic approach for diet-induced insulin resistance.

It is interesting to note that treatment with ASO significantly reduced body weight gain, particularly body fat mass, in both HFD-fed and *ob/ob* mice. Although our previous studies have shown that knockout of *Lpcat3* in the liver increases energy expenditure though FGF21 induction (15), there was no difference in energy expenditure between *Lpcat3*-ASO and control-ASO treated mice. Previous research has demonstrated that *Lpcat3* deficiency impairs lipid absorption in the intestine (13), which likely contributes to less

body weight gain on HFD. In *ob/ob* mice, we found that knockdown of *Lpcat3* increased the expression of lipolytic enzymes in adipose tissues and reduced RER, suggesting that Lpcat3-ASO injected mice predominantly utilize fat as energy source. However, it remains to be determined how changes in membrane phospholipid composition affects energy, lipid and glucose metabolism in adipose tissues.

In summary, our data demonstrate that targeting *Lpcat3* expression improves obesity and insulin resistance in both HFD-fed and genetic *ob/ob* models, which could be a novel therapeutic approach to treat obesity and insulin resistance.

Limitation of the study

In our study, we assessed the therapeutic potential of acute *Lpcat3* depletion against insulin resistance in several mouse models. Although both liver-specific and whole-body knockdown of *Lpcat3* improved insulin sensitivity, the transition to future clinical applications requires further investigation, given the difference between mouse models and human patients. Furthermore, the physiological function of LPCAT3 remains unclear in other organs such as brain and pancreas. Therefore, potential side effects associated with whole-body *Lpcat3* inhibition, although not evident in our study, necessitate comprehensive characterization and scrutiny.

Acknowledgements.

The authors thank Karen Doty at the Comparative Biosciences Histology Laboratory for technical support with histology analysis.

Funding.

This work was supported by grants from National Institute of Health (NIH) (DK114373 and DK128167 to B.W.), start-up funds from the University of Illinois at Urbana-Champaign (B.W.) and Burnsides Laboratory Research Fund (B.W.).

Data availability

The data that support the findings of this study are available in the results of this article. Original data or any additional information that support the findings of this study will be available on request from the corresponding author.

Reference

1. Magliano DJ, and Boyko EJ (2021) In IDF DIABETES ATLAS, Brussels
2. Magliano DJ, Islam RM, Barr ELM, Gregg EW, Pavkov ME, Harding JL, Tabesh M, Koye DN, and Shaw JE (2019) Trends in incidence of total or type 2 diabetes: systematic review. BMJ 366, l5003 [PubMed: 31511236]
3. Zheng Y, Ley SH, and Hu FB (2018) Global aetiology and epidemiology of type 2 diabetes mellitus and its complications. Nat Rev Endocrinol 14, 88–98 [PubMed: 29219149]
4. Brown MS, and Goldstein JL (2008) Selective versus total insulin resistance: a pathogenic paradox. Cell Metab 7, 95–96 [PubMed: 18249166]
5. Samuel VT, and Shulman GI (2016) The pathogenesis of insulin resistance: integrating signaling pathways and substrate flux. J Clin Invest 126, 12–22 [PubMed: 26727229]
6. Titchenell PM, Lazar MA, and Birnbaum MJ (2017) Unraveling the Regulation of Hepatic Metabolism by Insulin. Trends Endocrinol Metab 28, 497–505 [PubMed: 28416361]

7. Wang B, and Tontonoz P (2019) Phospholipid Remodeling in Physiology and Disease. Annu Rev Physiol 81, 165–188 [PubMed: 30379616]
8. van Meer G, Voelker DR, and Feigenson GW (2008) Membrane lipids: where they are and how they behave. Nat Rev Mol Cell Biol 9, 112–124 [PubMed: 18216768]
9. Lands WE (1958) Metabolism of glycerolipides; a comparison of lecithin and triglyceride synthesis. J Biol Chem 231, 883–888 [PubMed: 13539023]
10. Zhao Y, Chen YQ, Bonacci TM, Bredt DS, Li S, Bensch WR, Moller DE, Kowala M, Konrad RJ, and Cao G (2008) Identification and characterization of a major liver lysophosphatidylcholine acyltransferase. J Biol Chem 283, 8258–8265 [PubMed: 18195019]
11. Rong X, Albert CJ, Hong C, Duerr MA, Chamberlain BT, Tarling EJ, Ito A, Gao J, Wang B, Edwards PA, Jung ME, Ford DA, and Tontonoz P (2013) LXRs regulate ER stress and inflammation through dynamic modulation of membrane phospholipid composition. Cell Metab 18, 685–697 [PubMed: 24206663]
12. Rong X, Wang B, Dunham MM, Hedde PN, Wong JS, Gratton E, Young SG, Ford DA, and Tontonoz P (2015) Lpcat3-dependent production of arachidonoyl phospholipids is a key determinant of triglyceride secretion. Elife 4
13. Wang B, Rong X, Duerr MA, Hermanson DJ, Hedde PN, Wong JS, Vallim TQ, Cravatt BF, Gratton E, Ford DA, and Tontonoz P (2016) Intestinal Phospholipid Remodeling Is Required for Dietary-Lipid Uptake and Survival on a High-Fat Diet. Cell Metab 23, 492–504 [PubMed: 26833026]
14. Rong X, Wang B, Palladino EN, de Aguiar Vallim TQ, Ford DA, and Tontonoz P (2017) ER phospholipid composition modulates lipogenesis during feeding and in obesity. J Clin Invest 127, 3640–3651 [PubMed: 28846071]
15. Tian Y, Mehta K, Jellinek MJ, Sun H, Lu W, Shi R, Ingram K, Friedline RH, Kim JK, Kemper JK, Ford DA, Zhang K, and Wang B (2023) Hepatic Phospholipid Remodeling Modulates Insulin Sensitivity and Systemic Metabolism. Adv Sci (Weinh), e2300416
16. Ferrara PJ, Rong X, Maschek JA, Verkerke AR, Siripoksup P, Song H, Green TD, Krishnan KC, Johnson JM, Turk J, Houmard JA, Lusis AJ, Drummond MJ, McClung JM, Cox JE, Shaikh SR, Tontonoz P, Holland WL, and Funai K (2021) Lysophospholipid acylation modulates plasma membrane lipid organization and insulin sensitivity in skeletal muscle. J Clin Invest 131
17. Tschop MH, Speakman JR, Arch JR, Auwerx J, Bruning JC, Chan L, Eckel RH, Farese RV Jr., Galgani JE, Hambly C, Herman MA, Horvath TL, Kahn BB, Kozma SC, Maratos-Flier E, Muller TD, Munzberg H, Pfluger PT, Plum L, Reitman ML, Rahmouni K, Shulman GI, Thomas G, Kahn CR, and Ravussin E (2011) A guide to analysis of mouse energy metabolism. Nat Methods 9, 57–63 [PubMed: 22205519]
18. Muller TD, Klingenspor M, and Tschop MH (2021) Revisiting energy expenditure: how to correct mouse metabolic rate for body mass. Nat Metab 3, 1134–1136 [PubMed: 34489606]
19. Tian Y, Jellinek MJ, Mehta K, Seok SM, Kuo SH, Lu W, Shi R, Lee R, Lau GW, Kemper JK, Zhang K, Ford DA, and Wang B (2023) Membrane phospholipid remodeling modulates nonalcoholic steatohepatitis progression by regulating mitochondrial homeostasis. Hepatology doi: 10.1097/HEP.0000000000000375.
20. Shi R, Lu W, Tian Y, and Wang B (2023) Intestinal SEC16B modulates obesity by regulating chylomicron metabolism. Mol Metab 70, 101693 [PubMed: 36796587]
21. Bligh EG, and Dyer WJ (1959) A rapid method of total lipid extraction and purification. Can J Biochem Physiol 37, 911–917 [PubMed: 13671378]
22. Demarco VG, Ford DA, Henriksen EJ, Aroor AR, Johnson MS, Habibi J, Ma L, Yang M, Albert CJ, Lally JW, Ford CA, Prasannarong M, Hayden MR, Whaley-Connell AT, and Sowers JR (2013) Obesity-related alterations in cardiac lipid profile and nondipping blood pressure pattern during transition to diastolic dysfunction in male db/db mice. Endocrinology 154, 159–171 [PubMed: 23142808]
23. Han X, and Gross RW (2005) Shotgun lipidomics: electrospray ionization mass spectrometric analysis and quantitation of cellular lipidomes directly from crude extracts of biological samples. Mass Spectrom Rev 24, 367–412 [PubMed: 15389848]

24. Shulman GI (2000) Cellular mechanisms of insulin resistance. J Clin Invest 106, 171–176 [PubMed: 10903330]

25. Petersen MC, and Shulman GI (2018) Mechanisms of Insulin Action and Insulin Resistance. Physiol Rev 98, 2133–2223 [PubMed: 30067154]

26. James DE, Stockli J, and Birnbaum MJ (2021) The aetiology and molecular landscape of insulin resistance. Nat Rev Mol Cell Biol 22, 751–771 [PubMed: 34285405]

27. Yaribeygi H, Farrokhi FR, Butler AE, and Sahebkar A (2019) Insulin resistance: Review of the underlying molecular mechanisms. J Cell Physiol 234, 8152–8161 [PubMed: 30317615]

28. Samuel VT, and Shulman GI (2012) Mechanisms for insulin resistance: common threads and missing links. Cell 148, 852–871 [PubMed: 22385956]

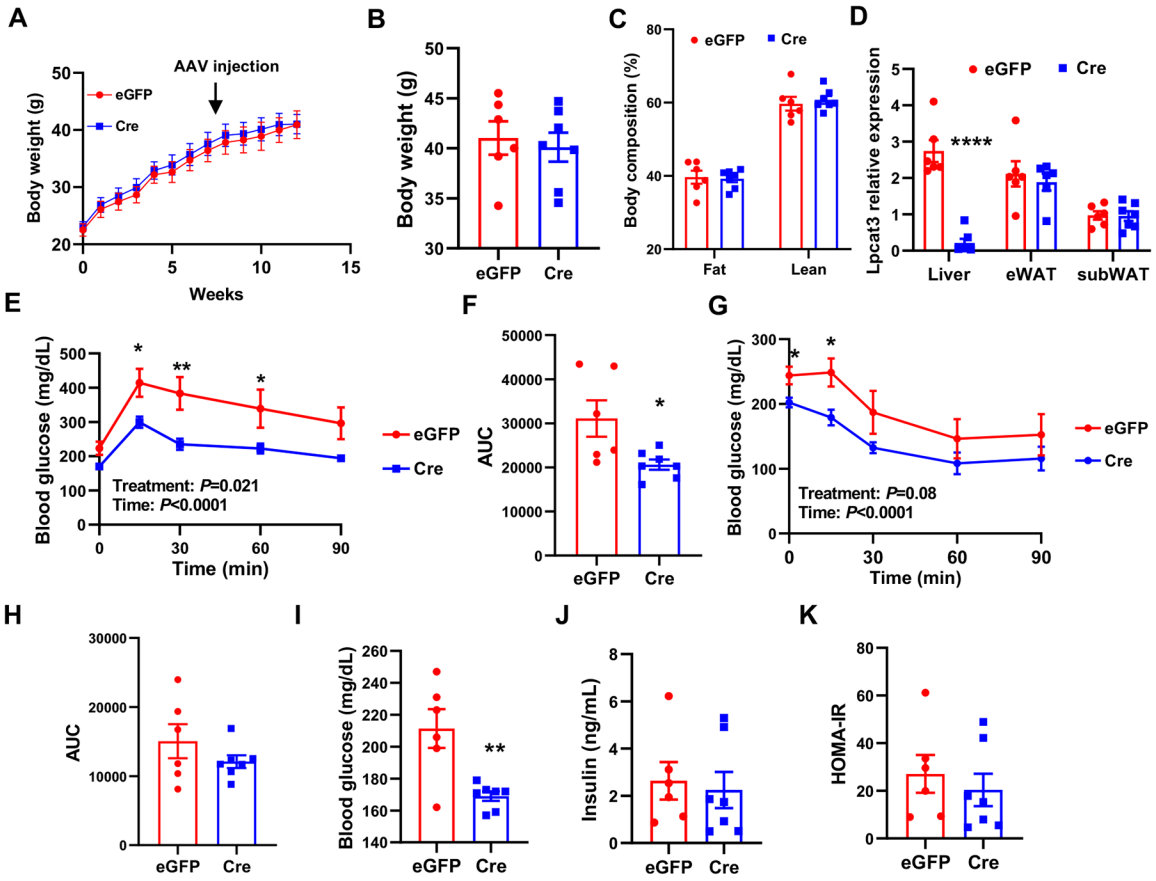

Figure 1. Acute deletion of *Lpcat3* in the liver improves insulin sensitivity in HFD-fed mice.

A. Growth curve of *Lpcat3*$^{fl/fl}$ mice fed HFD for 8 weeks followed by retro-orbital injection with AAV8-TBG-eGFP or AAV8-TBG-iCre (n=6–7/group).

B-C. Body weight and body composition in AAV injected HFD fed mice.

D. Lpcat3 mRNA levels in the liver and adipose tissues in AAV injected HFD fed mice.

E-H. GTT, ITT and area under the curve (AUC) analysis in HFD-fed *Lpcat3*$^{fl/fl}$ mice injected with AAV8-TBG-eGFP or AAV8-TBG-iCre (n=6–7/group).

I-K. Fasting blood glucose (I), serum insulin levels (J) and HOMA-IR (K) of HFD-fed *Lpcat3*$^{fl/fl}$ mice injected with AAV8-TBG-eGFP or AAV8-TBG-iCre (n=6–7/group).

Data are represented as means ± SEM. Statistical analysis was performed with two-way ANOVA (C, E and G) and Student's t test (B, D, F, H-K). *$P < 0.05$, **$P < 0.01$, ****$P < 0.0001$.

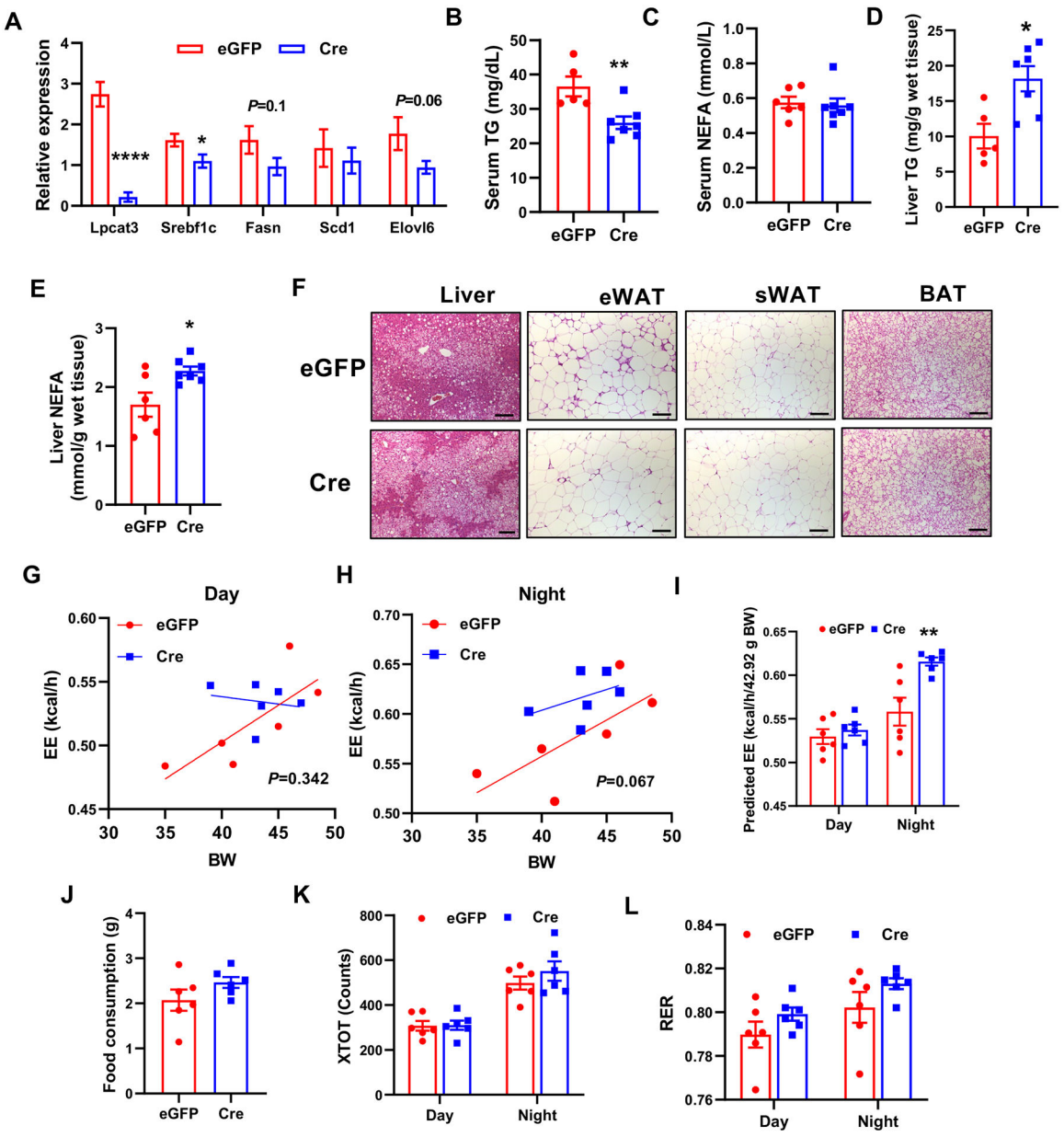

Figure 2. Acute deletion of *Lpcat3* in the liver improves hypertriglyceridemia in HFD-fed mice.

A. Expression of selected genes in the livers of HFD-fed *Lpcat3*$^{fl/fl}$ mice injected with AAV8-TBG-eGFP or AAV8-TBG-iCre (n=6–7/group).

B-E. Serum triglyceride (B) and NEFA (C) levels and liver triglyceride (D) and NEFA (E) levels of HFD-fed *Lpcat3*$^{fl/fl}$ mice injected with AAV8-TBG-eGFP or AAV8-TBG-iCre.

F. Representative histology of liver, epididymal white adipose tissue (eWAT), subcutaneous white adipose tissue (sWAT) from HFD-fed *Lpcat3*$^{fl/fl}$ mice injected with AAV8-TBG-eGFP or AAV8-TBG-iCre. Scale bar: 100 μm.

G-H. Energy expenditure (EE) analyzed by regression analysis of covariance (ANCOVA).

I. EE estimated by univariate generalized linear model (GLM) with body mass set to 42.92 g (average body mass of AAV8-TBG-eGFP or AAV8-TBG-iCre injected mice on HFD).

J-L. Food consumption (J), physical activity (K) and respiratory exchange ratio (RER) (L) in HFD-fed *Lpcat3*$^{fl/fl}$ mice injected with AAV8-TBG-eGFP or AAV8-TBG-iCre.
Data are presented as means ± SEM. Statistical analysis was performed with Student's t test (A-E, J), ANCOVA (G-H), and two-way ANOVA (I, K, L). *$P < 0.05$, **$P < 0.01$, ****$P < 0.0001$.

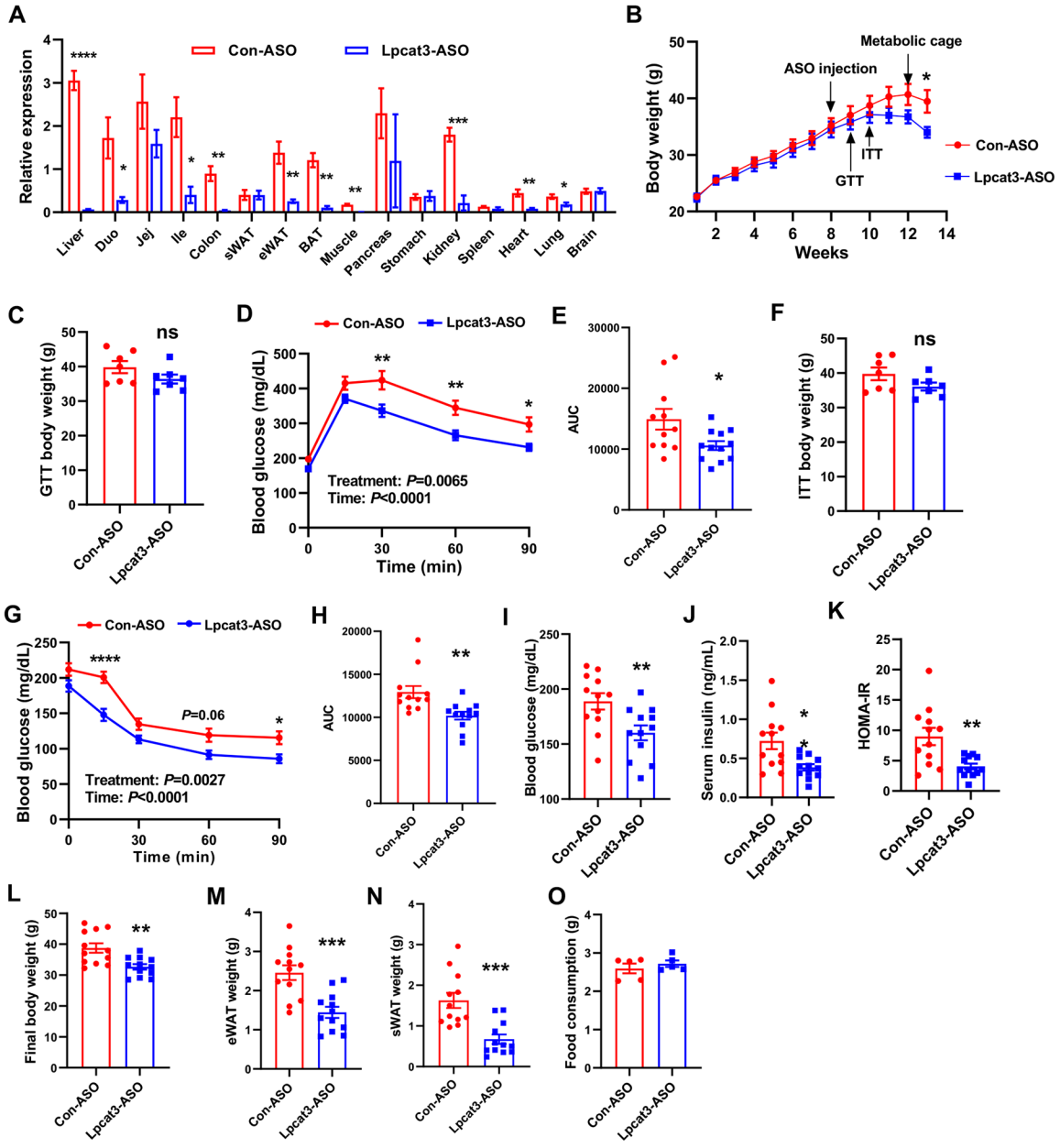

Figure 3. Whole body silencing *Lpcat3* expression improves HFD-induced obesity and insulin resistance.

A. Expression of *Lpcat3* in different tissues of chow diet-fed *C57BL/6* mice subcutaneously injected with control and *Lpcat3* targeting ASOs (n=5–8/group).

B. Growth curve of *C57BL/6* mice fed HFD for 8 weeks followed by subcutaneous injection with control (Con-ASO) or *Lpcat3* targeting ASO (*Lpcat3*-ASO) (n=12/group).

C and F. Mouse body weight when GTT and ITT were performed.

D-E and G-H. GTT, ITT and area under the curve (AUC) analysis in HFD-fed *C57BL/6* mice injected with Con-ASO or *Lpcat3*-ASO (n=11–12/group).

I-K. Fasting blood glucose (**I**), serum insulin levels (**J**) and HOMA-IR (**K**) of HFD-fed *C57BL/6* mice injected with Con-ASO or *Lpcat3*-ASO.

L-N. Final body weight (L), eWAT weight (M) and sWAT weight (N) of HFD-fed *C57BL/6* mice injected with Con-ASO or *Lpcat3*-ASO.

O. Food consumption of HFD-fed *C57BL/6* mice injected with Con-ASO or *Lpcat3*-ASO. Data are presented as means ± SEM. Statistical analysis was performed with Student's t test (A-C, E-F, H-O), and two-way ANOVA (D and G). *$P < 0.05$, **$P < 0.01$, ***$P < 0.001$, ****$P < 0.0001$.

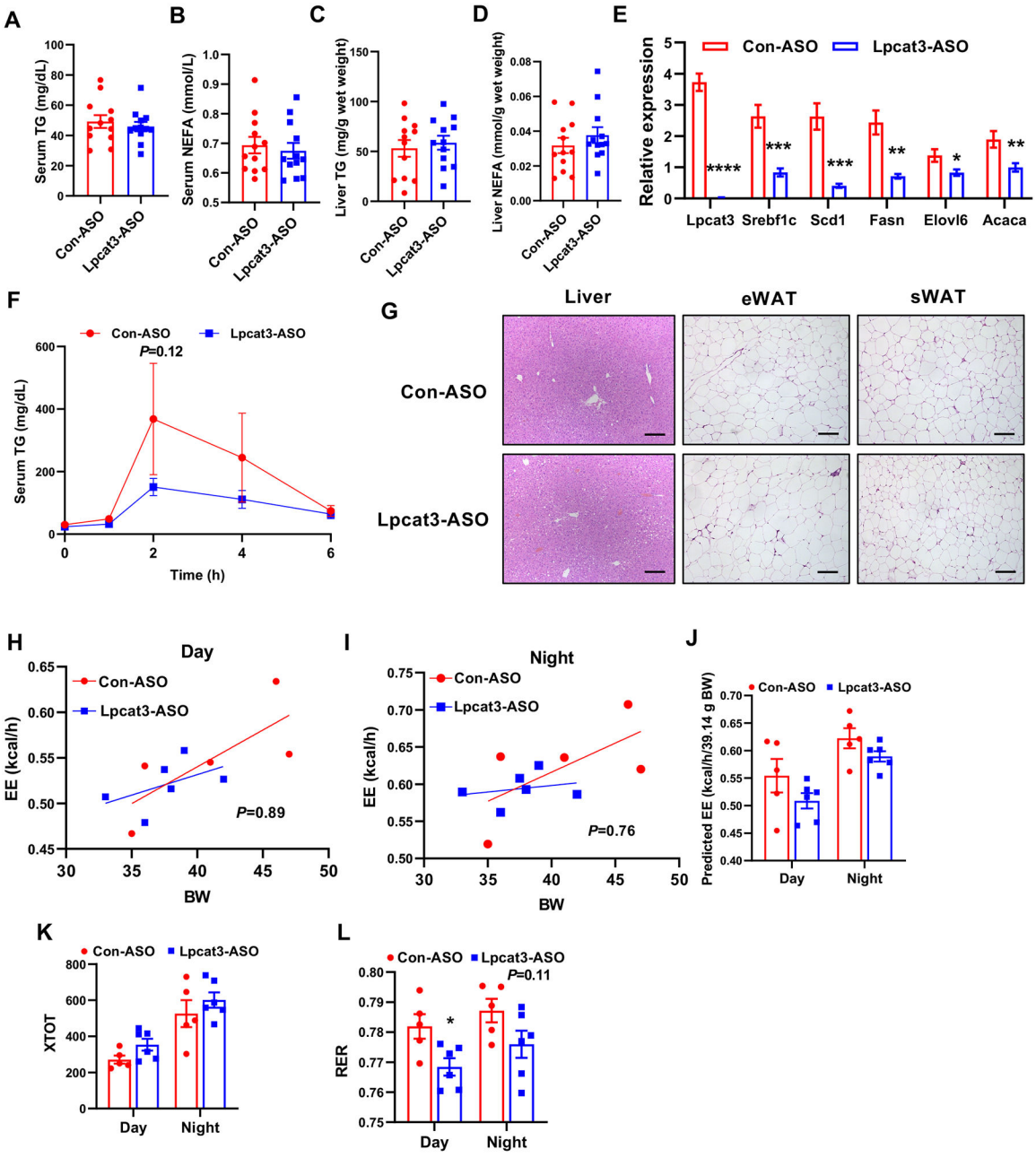

Figure 4. Whole body silencing *Lpcat3* expression has no effect on lipid and energy metabolism in HFD-fed mice.

A-D. Serum triglyceride (A) and NEFA (B) levels and liver triglyceride (C) and NEFA (D) levels of HFD-fed *C57BL/6* mice injected with Con-ASO or *Lpcat3*-ASO.

E. Expression of selected genes in the livers of HFD-fed *C57BL/6* mice injected with Con-ASO or *Lpcat3*-ASO (n=12/group).

F. Postprandial lipid absorption analysis in HFD-fed *C57BL/6* mice injected with Con-ASO or *Lpcat3*-ASO (n=4–5/group).

G. Representative histology of liver, eWAT and sWAT from HFD-fed *C57BL/6* mice injected with Con-ASO or *Lpcat3*-ASO. Scale bar: 100 μm.

H-I. Energy expenditure (EE) analyzed by regression analysis of covariance (ANCOVA).
J. EE estimated by univariate generalized linear model (GLM) with body mass set to 39.14 g (average body mass of Con-ASO or *Lpcat3*-ASO injected mice on HFD).
K-L. Physical activity (K) and respiratory exchange ratio (RER) (L) in HFD-fed *Lpcat3*$^{fl/fl}$ mice injected with Con-ASO or *Lpcat3*-ASO.
Data are presented as means ± SEM. Statistical analysis was performed with Student's t test (A-E), ANCOVA (H-I), and two-way ANOVA (F, J-L). *$P < 0.05$, **$P < 0.01$, ***$P < 0.001$, ****$P < 0.0001$.

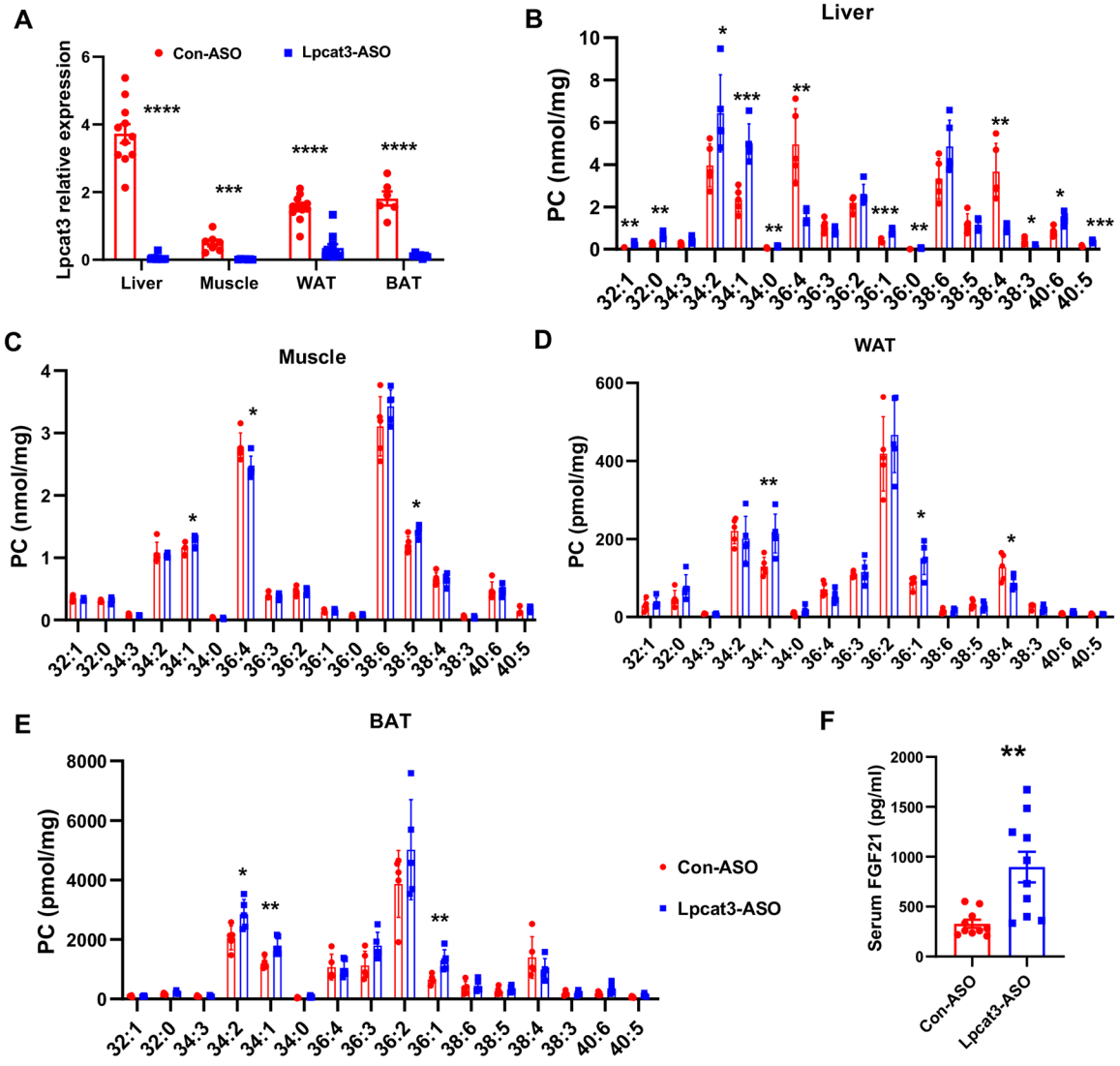

Figure 5. Whole-body silencing *Lpcat3* expression alters phospholipid composition in metabolic organs.

A. Expression of *Lpcat3* in different tissues of HFD-fed *C57BL/6* mice subcutaneously injected with control and *Lpcat3* targeting ASOs (n=6–12/group).

B-E. PC composition in the liver, muscle, WAT and BAT of HFD-fed mice injected with ASO (n=5/group).

F. Serum FGF21 levels in HFD-fed mice injected with ASO (n=10/group).

Data are presented as means ± SEM. Statistical analysis was performed with Student's t test. $*P < 0.05$, $**P < 0.01$, $***P < 0.001$, $****P < 0.0001$.

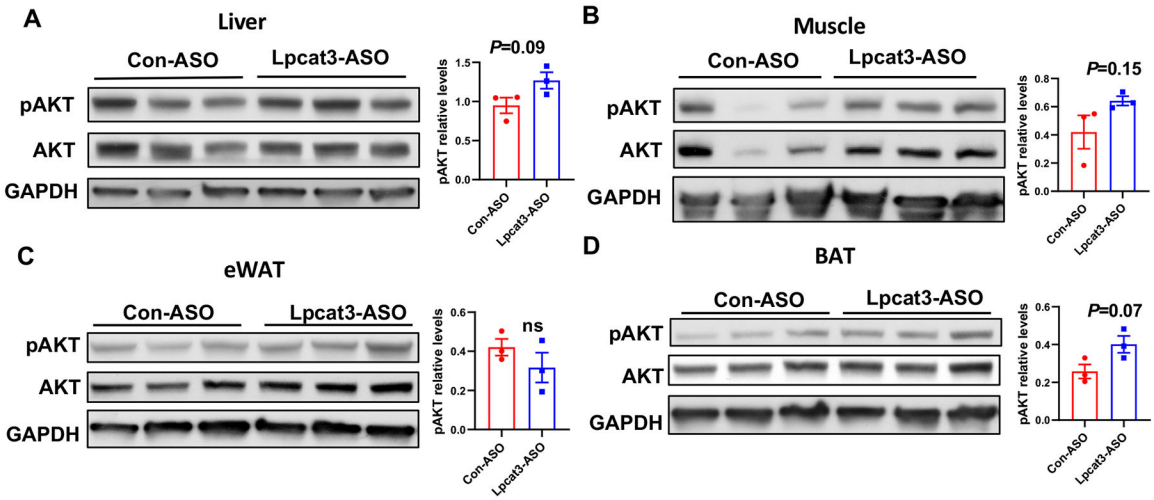

Figure 6. Whole-body silencing *Lpcat3* expression enhances insulin signaling in the liver and BAT.

A-D. Western blot analysis of p-AKT levels in the liver, muscle, WAT and BAT from ASO treated HFD fed mice. Mice were fasted overnight and retro-orbitally injected with insulin (1 U/kg BW) for 10 min.

Data are presented as means ± SEM. Statistical analysis was performed with Student's t test.

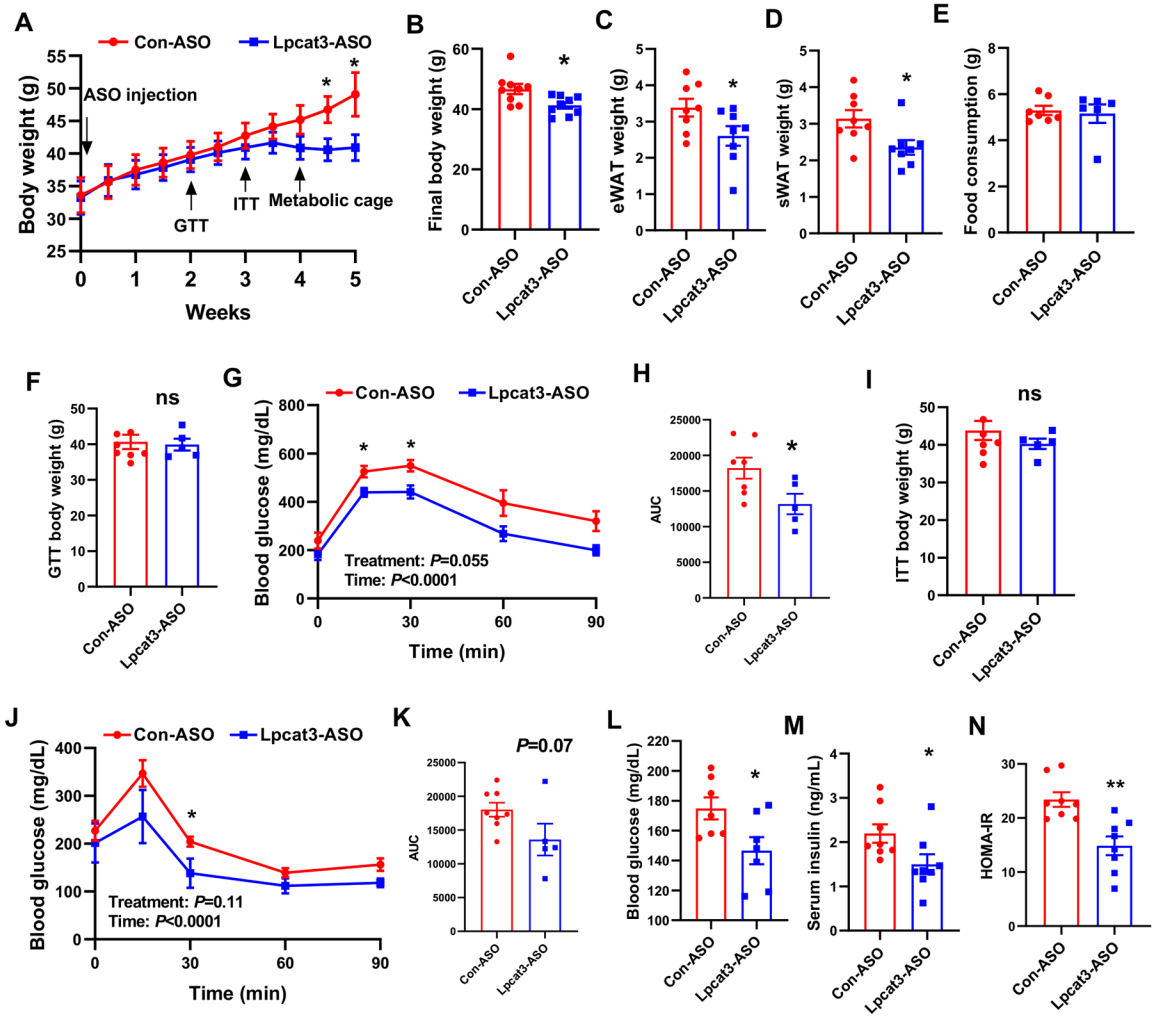

Figure 7. Global suppression of *Lpcat3* ameliorates obesity and insulin resistance in *ob/ob* mice.

A. Growth curve of *ob/ob* mice injected with Con-ASO or *Lpcat3*-ASO (n=8/group).

B-D. Body weight (B), eWAT weight (C) and sWAT weight (D) of *ob/ob* mice injected with Con-ASO or *Lpcat3*-ASO.

E. Daily food consumption of *ob/ob* mice injected with Con-ASO or *Lpcat3*-ASO.

F-K. GTT, ITT and area under the curve (AUC) analysis in *ob/ob* mice injected with Con-ASO or *Lpcat3*-ASO (n=5–8/group).

L-N. Fasting blood glucose (**L**), serum insulin levels (**M**) and HOMA-IR (**N**) of *ob/ob* mice injected with Con-ASO or *Lpcat3*-ASO.

Data are presented as means ± SEM. Statistical analysis was performed with Student's t test (A-F, H-I, K-N), and two-way ANOVA (G and J). **P* < 0.05, ***P* < 0.01.

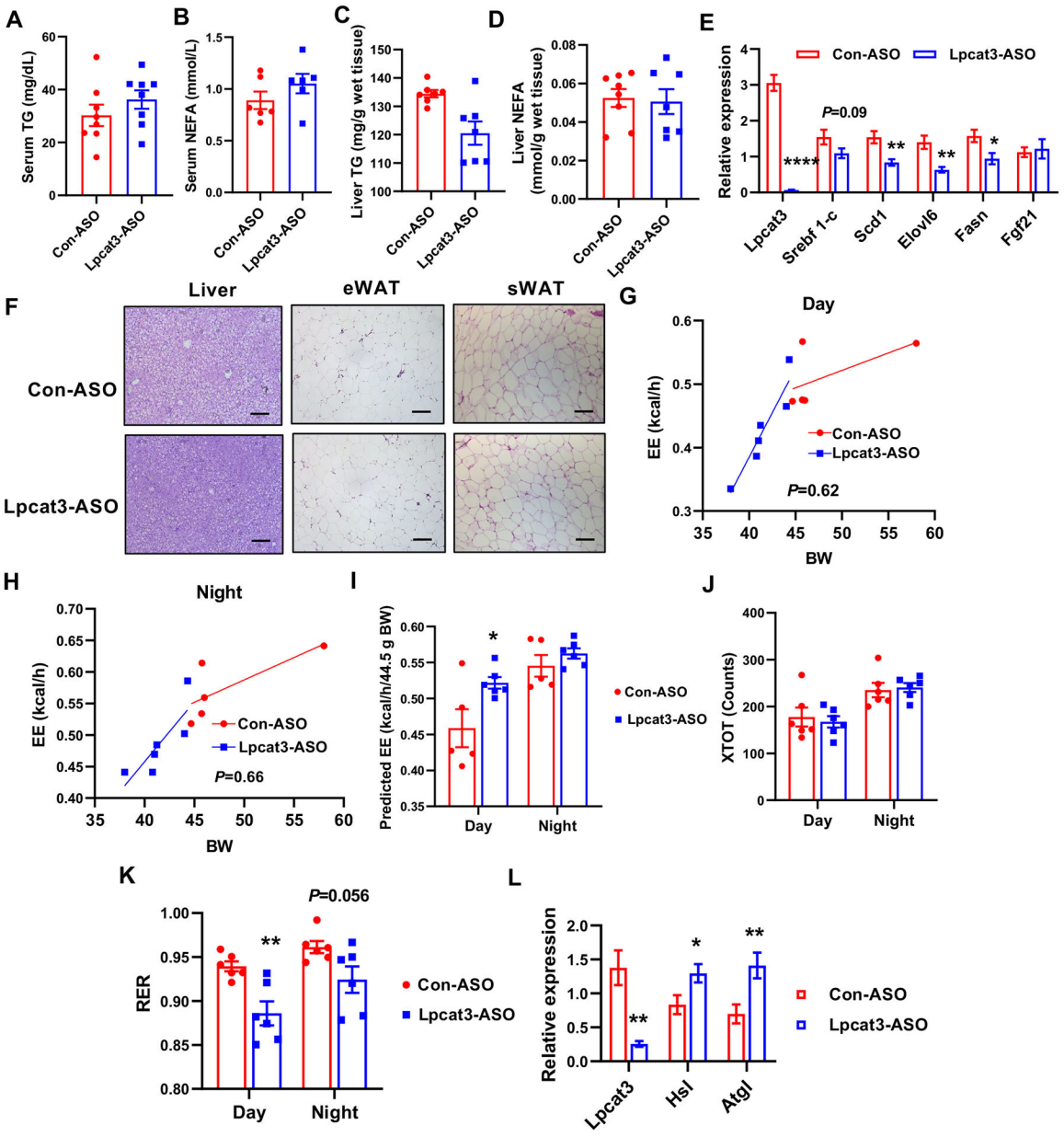

Figure 8. Global suppression of *Lpcat3* has no effect on lipid metabolism in *ob/ob* mice.

A-D. Serum triglyceride (**A**) and NEFA (**B**) levels and liver triglyceride (**C**) and NEFA (**D**) levels of *ob/ob* mice injected with Con-ASO or *Lpcat3*-ASO.

E. Expression of selected genes in the livers of *ob/ob* mice injected with Con-ASO or *Lpcat3*-ASO (n=7–8/group).

F. Representative histology of liver, eWAT and sWAT from *ob/ob* mice injected with Con-ASO or *Lpcat3*-ASO. Scale bar: 100 μm.

G-H. Energy expenditure (EE) analyzed by regression analysis of covariance (ANCOVA).

I. EE estimated by univariate generalized linear model (GLM) with body mass set to 44.5 g (average body mass of Con-ASO or *Lpcat3*-ASO injected *ob/ob* mice).

J-K. Physical activity (J) and respiratory exchange ratio (RER) (K) in *ob/ob* mice injected with Con-ASO or *Lpcat3*-ASO.

L. Expression of *Lpcat3* and lipases in eWAT of *ob/ob* mice injected with Con-ASO or *Lpcat3*-ASO (n=7–8/group).

Data are presented as means ± SEM. Statistical analysis was performed with Student's t test (A-E), ANCOVA (G-H), and two-way ANOVA (I-K). $*P < 0.05$, $**P < 0.01$, $****P < 0.0001$.